Taylor & Francis
Taylor & Francis Group

Canadian Journal of Remote Sensing
Journal canadien de télédétection

ISSN: (Print) (Online) Journal homepage: https://www.tandfonline.com/loi/ujrs20

RADARSAT-2 Derived Glacier Velocities and Dynamic Discharge Estimates for the Canadian High Arctic: 2015–2020

Wesley Van Wychen , David Burgess , Will Kochtitzky , Natalija Nikolic , Luke Copland & Laurence Gray

To cite this article: Wesley Van Wychen , David Burgess , Will Kochtitzky , Natalija Nikolic , Luke Copland & Laurence Gray (2021): RADARSAT-2 Derived Glacier Velocities and Dynamic Discharge Estimates for the Canadian High Arctic: 2015–2020, Canadian Journal of Remote Sensing, DOI: 10.1080/07038992.2020.1859359

To link to this article: https://doi.org/10.1080/07038992.2020.1859359

Published online: 06 Jan 2021.

CANADIAN JOURNAL OF REMOTE SENSING
https://doi.org/10.1080/07038992.2020.1859359

Taylor & Francis
Taylor & Francis Group

RADARSAT-2 Derived Glacier Velocities and Dynamic Discharge Estimates for the Canadian High Arctic: 2015–2020

Estimations des vitesses et de la décharge dynamique des glaciers dans l'Extrême-Arctique canadien de 2015 à 2020 d'après les observations de RADARSAT-2

Wesley Van Wychen[a,b], David Burgess[c], Will Kochtitzky[b], Natalija Nikolic[a], Luke Copland[b], and Laurence Gray[b]

[a]Department of Geography and Environmental Management, University of Waterloo, 200 University Avenue West, Building EV-1, Waterloo, Ontario N2L 3G1, Canada; [b]Department of Geography, Environment and Geomatics, University of Ottawa, 60 University Pvt., Ottawa, Ontario K1N 6N5, Canada; [c]Natural Resources Canada, 601 Booth Street, Ottawa, Ontario K1A 0E8, Canada

ABSTRACT

RADARSAT-2 imagery collected each winter from 2015/2016 to 2019/2020 is used to quantify and characterize the variability in the motion of, and the discharge from, the major marine-terminating ice masses of the Queen Elizabeth Islands (QEI: Devon, Ellesmere and Axel Heiberg Islands) in the Canadian High Arctic. The majority of the glaciers did not experience significant variations in flow speeds over the observation period, and for most that did the variations are attributed to pulse and surge processes. However, there are exceptions where the velocity record indicates continued acceleration of the glaciers by processes that appear distinct from surging or pulsing, such as dynamic thinning. These include Trinity and Wykeham glaciers (Prince of Wales Icefield) and Belcher Glacier (Devon Ice Cap). The combination of surface velocities with ice thicknesses indicates that average ice discharge to the ocean for the QEI over the observation period was 2.78 ± 0.52 Gt a^{-1} (ranging between $\sim 2.37 \pm 0.48$ Gt a^{-1} and $\sim 3.20 \pm 0.55$ Gt a^{-1}), ~50% of which was channeled through the Trinity-Wykeham glacier basin alone. The results presented here, combined with those of previous studies, provide a comprehensive record of ice motion and discharge from the QEI between 2008 and 2020.

RÉSUMÉ

Des images recueillies par RADARSAT-2 dans l'Extrême-Arctique canadien chaque hiver de 2015–2016 à 2019–2020 ont permis de quantifier et de caractériser la variabilité du mouvement et de la décharge des principales masses glaciaires des îles de la Reine-Élisabeth (îles Devon, d'Ellesmere et Axel Heiberg) se jetant dans l'océan. Au cours de la période d'observation, la vitesse d'écoulement de la plupart des glaciers n'a pas connu d'importantes variations et, le cas échéant, la plupart de ces variations étaient attribuables à des processus d'impulsions et de poussées. Toutefois, il existe des exceptions où le relevé de la vitesse montre une accélération continue des glaciers causée par des processus qui semblent distincts de la poussée ou de l'impulsion, comme l'amincissement dynamique. Ces exceptions concernent notamment les glaciers Trinity et Wykeham (champ de glace Prince-de-Galles) et le glacier Belcher (calotte glaciaire Devon). Ensemble, les vitesses superficielles et les épaisseurs de la glace indiquent qu'au cours de la période d'observation, le débit moyen de la décharge des glaces dans l'océan depuis les îles de la Reine-Élisabeth était de $2{,}78 \pm 0{,}52$ Gt a^{-1} (soit de $\sim 2{,}37 \pm 0{,}48$ Gt a^{-1} à $\sim 3{,}20 \pm 0{,}55$ Gt a^{-1}), et qu'environ 50% de ce débit transitaient par le seul bassin des glaciers Trinity et Wykeham. Ces résultats, combinés à ceux d'études antérieures, offrent un relevé exhaustif du mouvement et de la décharge des glaces dans les îles de la Reine-Élisabeth entre 2008 et 2020.

ARTICLE HISTORY
Received 5 September 2020
Accepted 30 November 2020

CONTACT Wesley Van Wychen wvanwychen@uwaterloo.ca

Introduction

Canada contains the largest area of glaciated terrain outside of the Antarctic and Greenland ice sheets. Much of this vast terrain is located in remote locations with harsh environmental conditions and narrow annual windows when over ice travel is practical, which makes in situ glacier monitoring logistically difficult and expensive. Despite this, field campaigns to determine glacier mass balance at selected sites across northern Canada are undertaken on an annual basis, with some having records extending as far back as 1959 (Thomson et al. 2017). These in situ measurements, which do not include large dynamic glaciers that terminate in the ocean, are used to make inferences about regional glacier mass balance and how it is changing in a warming climate (Box et al. 2018). However, from a glacier dynamics monitoring perspective, much less is known about long-term, regional mean rates of glacier flow (e.g., over 5 years or more), although some work has occurred (Millan et al. 2017; Mortimer et al. 2018; Van Wychen et al. 2016, 2017). This is because in situ records of ice motion in Canada are exceedingly rare and because, historically, the remote sensing data required to measure glacier motion at regional scales was largely unavailable.

Despite the limitations in data availability, several studies since the 1960s have utilized optical imagery to determine rates and patterns of glacier motion within the Canadian High Arctic (e.g., Copland et al. 2003; Hattersley-Smith 1969; Williamson et al. 2008). However, the use of optical imagery to determine ice motion by these studies was typically limited by the availability of repeat cloud-free summer imagery, and mainly restricted to relatively large outlet glaciers with distinctive surface features (e.g., crevasses) that could be tracked. Synthetic Aperture RADAR (SAR) imagery has proved to be an attractive alternative to optical imagery to derive rates of glacier motion, given its ability to image in (nearly) all weather conditions and during the "Polar-night", as well as the fact that imagery could be ordered with relatively high confidence that it would be collected. Vachon et al. (1996) and Mattar et al. (1998) first showed the potential of resolving glacier velocities in Canada by applying interferometric processing to ERS-1/2 data collected in Alberta in the mid-1990s. Building upon these methods, Short and Gray (2004, 2005) applied a speckle-tracking method to SAR imagery from the RADARSAT-1 mission to show how this methodology could also be utilized to derive glacier dynamics in Nunavut. Building further on these efforts, Burgess et al. (2005) and Shepherd et al. (2007) both demonstrated how SAR data could be used to determine glacier dynamics at the regional scale in the Canadian Arctic by applying InSAR methods to ERS-1/2 data to derive ice motion for Devon Ice Cap. Together, these studies began to show the feasibility of undertaking a SAR-based glacier dynamics monitoring program that would provide a record of glacier flow for all ice masses in Canada. However, the major limitation to implementing such a large-scale glacier dynamics monitoring program was the lack of the regular collection of high-resolution SAR datasets necessary to complete the mapping.

The launch of the RADARSAT-2 (R2) mission in December 2007 ushered in a new era of SAR remote sensing in Canada and created the potential of a national glacier dynamics mapping program. For example, utilizing datasets collected by Government of Canada users in departments such as Natural Resources Canada, Parks Canada, and the Canadian Space Agency, Van Wychen et al. (2012, 2014) and Schaffer et al. (2017) demonstrated that monitoring regional scale glacier dynamics was possible for the Canadian High Arctic, with similar work subsequently undertaken for the ice masses of Yukon (Waechter et al. 2015) and Alberta and British Columbia (Van Wychen et al. 2018). Van Wychen et al. (2016, 2017) showed how R2 imagery collected each winter in the Canadian High Arctic could be used to determine how rates of ice motion within the region were changing, make inferences about the drivers of these changes, and calculate how much ice was lost to the ocean as dynamic discharge (thus helping to close regional mass balance estimates). These studies established baseline knowledge of ice motion for the nation and, together with other studies that have utilized similar imagery and methodologies (e.g., Millan et al. (2017) and Sánchez-Gámez and Navarro (2017) for Canadian High Arctic; Strozzi et al. (2017) and Van Wychen et al. (2015) for Baffin and Bylot Islands; Burgess et al. (2013) and Abe and Furuya (2015) for Alaska/Yukon), provide a robust record of surface velocities in Canada up to ~2016.

The launch of the RADARSAT Constellation Mission (RCM) in June 2019 represents a transition in SAR-based monitoring in Arctic Canada, with most applications transitioning from the use of R2 to RCM data to meet the needs of monitoring programs. This includes the annual glacier velocity mapping program initiated by earlier studies (Van Wychen et al. 2014, 2016, 2017; Waechter et al. 2015), which will be moving toward the use of RCM and Sentinel-1 (S1) data

and away from R2. However, the entire record of ice motion derived during the 2008–2020 "R2 era" over the Canadian Arctic has not yet been reported (here we define the R2 era as the period when this sensor provided the bulk of the data for the Government of Canada monitoring programs). Thus, the purpose of this study is to:

1. utilize imagery collected annually over the Queen Elizabeth Islands (QEI) to complete the record of glacier motion in the region for the past decade, and identify areas in which dynamic change occurred between winter 2008/09 and winter 2019/2020;
2. use updated and expanded measurements of ice thickness collected by NASA at the termini of tidewater terminating glaciers to calculate the amount of ice discharged to the ocean during the period from winter 2015/16 to winter 2019/2020 to provide updated estimates of regional dynamic discharge.

Study site and methods

The QEI (Devon, Axel Heiberg, and Ellesmere Islands; Figure 1a) contain ~107,000 km^2 of glacier ice, most of which is contained in major ice caps and icefields (identified in Figure 1a). R2 data for these ice masses have been collected in each winter since ~2011, and periodically since 2008. All R2 imagery from 2015/16 to 2019/20 that was processed for this study was acquired in Wide Fine beam mode (F0W1 to F0W3) in HH polarization and is summarized in Table 1. Image pairs were acquired on a 24-day repeat orbit, between December and April, when there is little likelihood of surface change (i.e., due to snowfall or melt) between images. This is necessary to ensure good coherence and therefore good results from the velocity determination method. Furthermore, although redistribution of snow can cause problems with coherence between image pairs, this issue is minimized in our data as most of the snowfall within the QEI occurs during the autumn.

Glacier velocities

To derive annual glacier velocities from the R2 data between 2015/16 and 2019/2020 we utilize a speckle-tracking method (Short and Gray 2004, 2005) which determines surface ice displacements from images collected with nearly identical imaging geometries (i.e., collected on the same R2 orbital path separated by 24 or 48 days). This methodology has been widely used in the Canadian Arctic (Van Wychen et al. 2012, 2014, 2015, 2016, 2017) and is capable of producing results similar to those derived from commercial software (Schellenberger et al. 2016). Because this speckle-tracking algorithm has been detailed in previous publications (Van Wychen et al. 2012, 2014, 2015, 2016, 2017; Waechter et al. 2015), readers are referred to those studies for an in-depth review of the methodology. We therefore only present a brief review of the methods here.

To ensure consistency in glacier velocities determined throughout the R2 era, we used identical processing parameters to those used by previous studies in the Canadian Arctic (Van Wychen et al. 2012, 2014, 2015, 2016, 2017). Specifically, we used image chip sizes of 101 pixels (~450 m) in azimuth and 61 pixels (~370 m) in range to determine displacements in both the azimuth and range directions of the images using a cross-correlation algorithm. Coarse registration of the images was completed automatically using orbital parameters provided in the image metadata. Next, we used the 1:250,000 Canadian Digital Elevation Dataset (CDED), which has a grid spacing of 100 m, to remove the topographic component of the slant range displacement to allow for the conversion into a ground range displacement. Finally, displacements were calibrated using nonmoving regions within the images (i.e., bedrock outcrops) and then standardized to annual values.

All assessments of the speckle-tracking results were completed manually using standard GIS software (ESRI ArcMap 10.7.1). Erroneous flow-induced displacements, which arise from mismatches in the cross-correlation algorithm, were identified by looking for vectors that deviated greatly in either magnitude or orientation from neighbors or that, for the case of nonsurge-type glaciers, were not aligned with glacier valley walls. Once identified, erroneous displacements were deleted from the vector dataset, and an Inverse Distance Weighting (IDW) interpolation was used to create a raster dataset of glacier velocities with 100 m grid spacing. The glacier velocity rasters were then mosaicked, using the lowest value for any overlapping pixel values from adjacent scenes, which provides a conservative estimate of surface velocity. They were then clipped to the extent of each ice mass using the outlines provided by the Randolph Glacier Inventory version 6.0 (RGI Consortium 2017). Finally, we used regions of the image that should be stationary (i.e., bedrock outcrops) in order to quantify velocity errors that arise from the misregistration of image chips

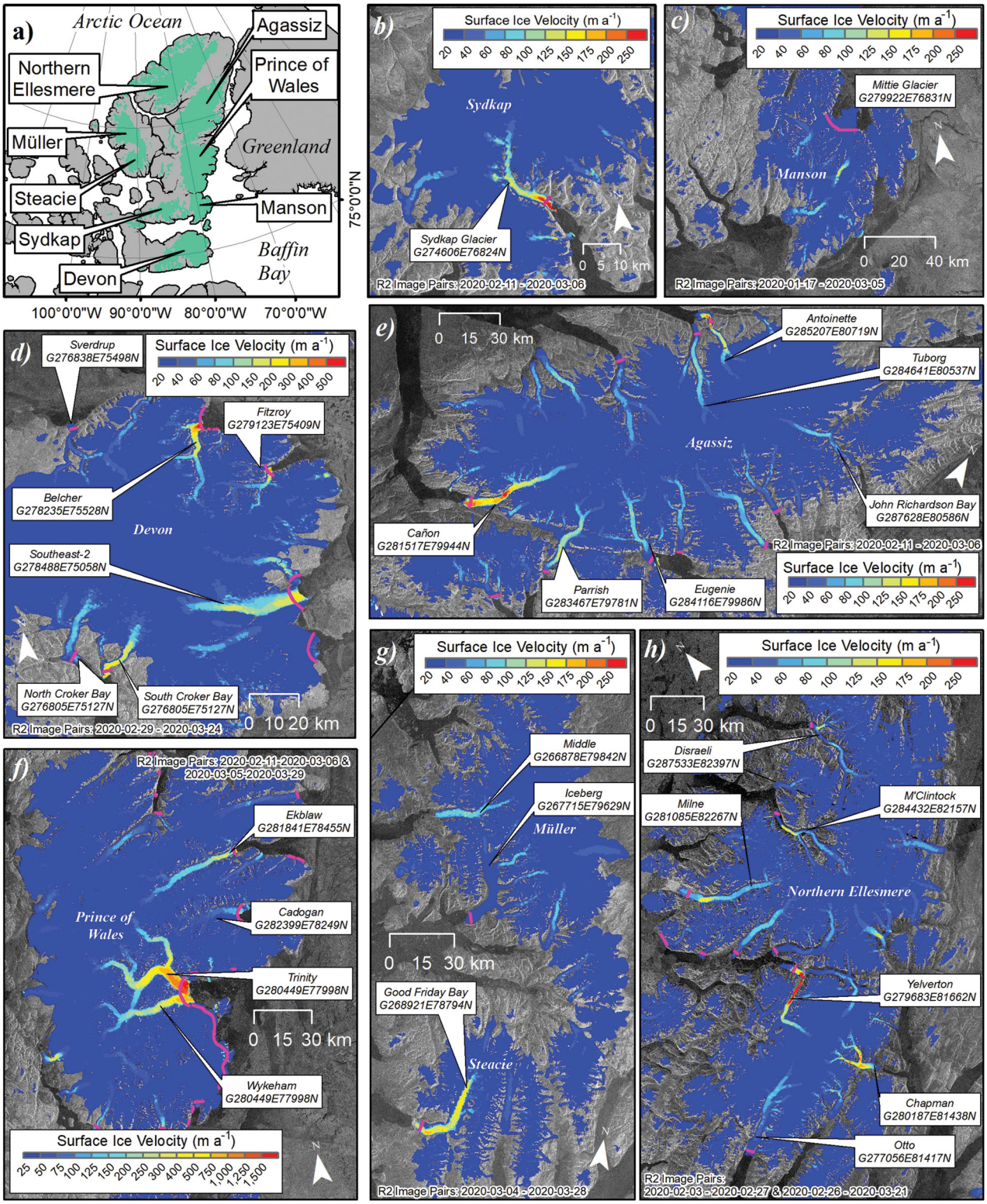

Figure 1. Study region and glacier velocities for winter 2019/2020 across the Queen Elizabeth Islands: (a) location of major ice masses; (b–h) surface ice motion for each of the major ice masses respectively: Sydkap Ice Cap, Manson Icefield, Devon Ice Cap, Agassiz Ice Cap, Prince of Wales Icefield, Steacie and Müller Ice Caps, Northern Ellesmere Icefield. Major glaciers are labeled. Note the difference in velocity scale between figure parts. Magenta lines at the termini of outlet glaciers denote the locations of flux gates used to calculate ice discharge.

Table 1. Radarsat-2 image pairs used to derive surface ice velocities in this study, together with mean error estimates extracted from stationary bedrock locations (numbers within brackets indicate the standard deviation).

Ice Mass	Winter	Image Date 1 (YYYY-MM-DD)	Image Date 2 (YYYY-MM-DD)	Beam Mode & Polarization	Bedrock Error (m a^{-1})
Northern Ellesmere	2015–2016	2016-01-07	2016-01-31	F0W1 – HH	7.54(5.99)
		2016-02-23	2016-03-18	F0W1 - HH	
	2016–2017	2017-03-13	2017-04-06	F0W1 – HH	6.06(6.37)
		2017-03-14	2017-04-07	F0W1 - HH	
	2017–2018	2018-01-19	2018-02-12	F0W1 – HH	7.25(6.26)
		2018-01-20	2018-02-13	F0W1 - HH	
	2018–2019	2018-12-22	2019-01-15	F0W1 – HH	5.64(4.64)
		2019-02-07	2019-03-03	F0W1 – HH	
		2019-02-08	2019-03-04	F0W1 - HH	
	2019–2020	2020-02-03	2020-02-27	F0W1 – HH	5.02(4.11)
		2020-02-26	2020-03-21	F0W1 - HH	
Agassiz	2015–2016	2016-03-03	2016-03-27	F0W1 - HH	6.00(5.96)
	2016–2017	2017-03-22	2017-04-15	F0W1 - HH	5.63(7.50)
	2017–2018	2017-12-11	2018-01-04	F0W1 - HH	6.05(5.95)
	2018–2019	2019-01-23	2019-02-16	F0W1 - HH	5.77(5.07)
	2019–2020	2020-02-11	2020-03-06	F0W1 - HH	5.02(5.74)
Steacie and Müller	2015–2016	2016-02-06	2016-03-01	F0W2 - HH	6.87(6.10)
	2016–2017	2017-03-20	2017-04-13	F0W2 - HH	5.29(8.13)
	2017–2018	2018-01-02	2018-01-26	F0W2 - HH	4.06(6.06)
	2018–2019	2019-02-14	2019-03-10	F0W2 - HH	4.30(3.24)
	2019–2020	2020-03-04	2020-03-28	F0W2 - HH	4.81(3.15)
Prince of Wales	2015–2016	2016-01-14	2016-02-07	F0W3 – HH	5.23(6.14)
		2016-03-03	2016-03-27	F0W1 - HH	
	2016–2017	2017-02-25	2017-03-21	F0W3 – HH	4.86(5.39)
		2017-03-22	2017-04-15	F0W1 - HH	
	2017–2018	2018-01-04	2018-01-28	F0W1 - HH	4.05(3.58)
	2018–2019	2019-01-22	2019-02-15	F0W1 – HH	4.29(5.31)
		2019-01-23	2019-02-16	F0W3 - HH	
	2019–2020	2020-02-11	2020-03-06	F0W1 – HH	5.17(4.74)
		2020-03-05	2020-03-29	F0W3 - HH	
Sydkap	2015–2016	2016-02-08	2016-03-01	F0W1 - HH	4.88(4.50)
	2016–2017	2017-01-09	2017-02-02	F0W1 - HH	5.89(4.10)
	2017–2018	2018-01-04	2018-01-28	F0W1 - HH	4.67(4.79)
	2018–2019	2019-01-23	2019-02-16	F0W1 - HH	3.95(6.66)
	2019–2020	2020-02-11	2020-03-06	F0W1 - HH	4.72(6.05)
Manson	2015–2016	2016-01-14	2016-02-07	F0W3 - HH	4.65(4.15)
	2016–2017	2017-02-01	2017-02-25	F0W3 - HH	5.05(4.54)
	2017–2018	2018-01-03	2018-01-27	F0W3 - HH	5.85(6.67)
	2018–2019	2019-01-22	2019-02-15	F0W3 - HH	3.36(3.59)
	2019–2020	2020-01-17	2020-03-05	F0W3 - HH	2.98(2.40)
Devon	2015–2016	2016-02-02	2016-02-26	F0W1 – HH	5.03(3.58)
		2016-02-07	2016-03-02	F0W3 - HH	
	2016–2017	2017-01-03	2017-01-27	F0W1 – HH	5.45(4.08)
		2017-02-25	2017-03-21	F0W3 - HH	
	2017–2018	2017-12-29	2018-01-22	F0W1 - HH	5.50(4.74)
	2018–2019	2019-01-22	2019-02-15	F0W3 – HH	3.61(3.20)
		2019-02-10	2019-03-06	F0W1 - HH	
	2019–2020	2020-02-29	2020-03-24	F0W1 - HH	5.27(4.30)

All Radarsat-2 imagery was acquired as Wide Fine data (beam modes identified in table) in 'HH' polarization (F0W1 imagery spans incidence angles (deg) from 20.4 in near range to 31.9 in far range and has a nominal pixel resolution of 14.9 m in near range and 9.9 m in far range, F0W2 imagery spans incidence angles (deg) from 30.6 in near range to 39.5 in far range and has a nominal pixel resolution of 10.2 m in near range and 8.2 m in far range, and F0W3 imagery spans incidence angles (deg) from 38.7 in near range to 45.3 in far range and has a nominal pixel resolution of 8.3 m in near range and 7.3 m in far range).

(Table 1 provides the error analysis for each ice mass in each year of observation).

In order to identify, quantify and characterize the dynamic variability over the period 2008–2020 we compared our 2015/16–2019/20 results with those previously derived by Van Wychen et al. (2016) for the period 2008/09–2014/15, by extracting centerline velocities from each major glacier for all years with available R2-derived surface velocity data. All centerlines were manually drawn using cloud-free Landsat-8 imagery to guide the delineation. Surface velocities were extracted every 50 m along the glacier centerline beginning at the glacier front and ending up-glacier where variations in ice motion were negligible.

Dynamic Discharge calculations

We calculated the ice flux for every major tidewater-terminating glacier in the study area by combining thickness measurements (described more fully in the next paragraph) with our velocity results. We manually drew fluxgates as perpendicular to flow as

possible, depending on the availability of ice thickness observations. We then calculated the ice flux along 64 tidewater terminating glaciers (glacier width defined by the RGI Consortium (2017)), totaling ~285 km of fluxgates (shown as black lines at the fronts of tidewater glaciers in Figure 1b–h). We created points along our flux gates every 25 m (referred to as flux point locations below) to sample velocity and thickness data products for use in the flux calculations. While the flux point locations are 25 m apart, we adjusted the width of the ice column that they represent for the flux calculations in cases where fluxgates were not perpendicular to flow, using the difference between velocity direction and fluxgate orientation.

For thickness observations, we mainly used CReSIS radar tomography observations that are available in ~3 km wide swaths from NASA's 2014 Operation IceBridge campaign (Allen 2013). These data covered 68.1% of our flux point locations. For 21.1% of our flux point locations we used observations from the GlaThiDa 3.0.3 dataset (GlaThiDa Consortium 2019), composed mostly of Operation IceBridge thickness observations in the Canadian Arctic, using the average of all GlaThiDa data points within 100 m of each flux point. For the remaining 10.8% of the flux point dataset we used interpolated ice thickness estimates based on centerline measurements and the assumption of a U-shaped valley (see equation 3 in Van Wychen et al. 2014). Most of these centerline measurements came from GlaThiDa, with the exception of two small glaciers on the eastern portion of Devon Island (East-5 and East-6) which were originally reported by Dowdeswell et al. (2004). For this we determined the centerline thickness by taking the average depth of the middle 100–125 m of the glacier (depending on whether there was an even or odd number of flux points along a flux gate). The only exception is the eastern side of Mittie Glacier, where we used the GlaThiDa observations 450 m east of the centerline as our centerline depth, as these are the only observations available. In some cases, glacier outlines provided by RGI 6 terminate in areas where two tributaries merge or have two spatially distinct termini. In these circumstances, we modeled the thickness separately for each valley, despite the fact that the RGI 6 outlines consider them to be a single glacier basin.

Uncertainty

To provide an estimate of the uncertainty in our estimates of cross-sectional ice thicknesses derived from interpolation of the centerline measurements, we modeled the thickness from locations for which we had data from a complete fluxgate. We find that our interpolated ice thickness is an average of 7.7% thicker than the observed thickness where observations exist. Further, we did not apply a correction factor to the flux gate ice thickness measurements to account for changes in thickness over time due to surface melt and runoff, or dynamic processes. There is a general thinning of ice masses in the CAA (Mortimer et al. 2018), but due to the lack of comprehensive measurements at the fronts of most tidewater glaciers in the region it is impossible to accurately bound correction values for individual glaciers, and doing so might introduce greater uncertainty to measurements.

The perpendicularity to the flow of each fluxgate also contributes to the overall uncertainty. We assume a 10° uncertainty in flow direction for the corrections of flux point length used to account for any non-perpendicular ice motion, which is incorporated into our overall uncertainty. This was not possible where ice motion is slow (< 25 m a^{-1}) due to poor flow direction information provided by the radar imaging geometry, or near glacier margins. In these cases, we assume our flux points could be as much as 45° away from perpendicular to flow, so we broaden our uncertainty to account for this.

Results and discussion

General pattern of ice motion in the QEI (winter 2015/2016–2019/2020)

Figure 1 presents the surface motion for all ice masses of the QEI in winter 2019/2020, with the broad pattern consistent with the other years investigated (2015/16 to 2018/19), and with previous studies that have determined glacier motion in the region (Millan et al. 2017; Van Wychen et al. 2014; 2016, 2017). In general, ice motion is slow within the interior regions of all ice masses (<20 m a^{-1}), where ice is presumed to be largely frozen to its bed and flowing due to internal deformation alone (Van Wychen et al. 2012) although the discovery of hypersaline subglacial lakes under portions of Devon Ice Cap likely means that ice is not frozen to the bed in all interior regions (Rutishauser et al. 2018). Velocities tend to increase, reaching typical speeds of 50–100 m a^{-1}, as ice is channeled into valleys which act as conduits that bring ice from interior regions to the margins. Ground- and aircraft- based ice penetrating RADAR measurements indicate that these large outlet valleys are generally incised deeply into bedrock (see Figure 8 in Dowdeswell et al. (2004) as an example). As a

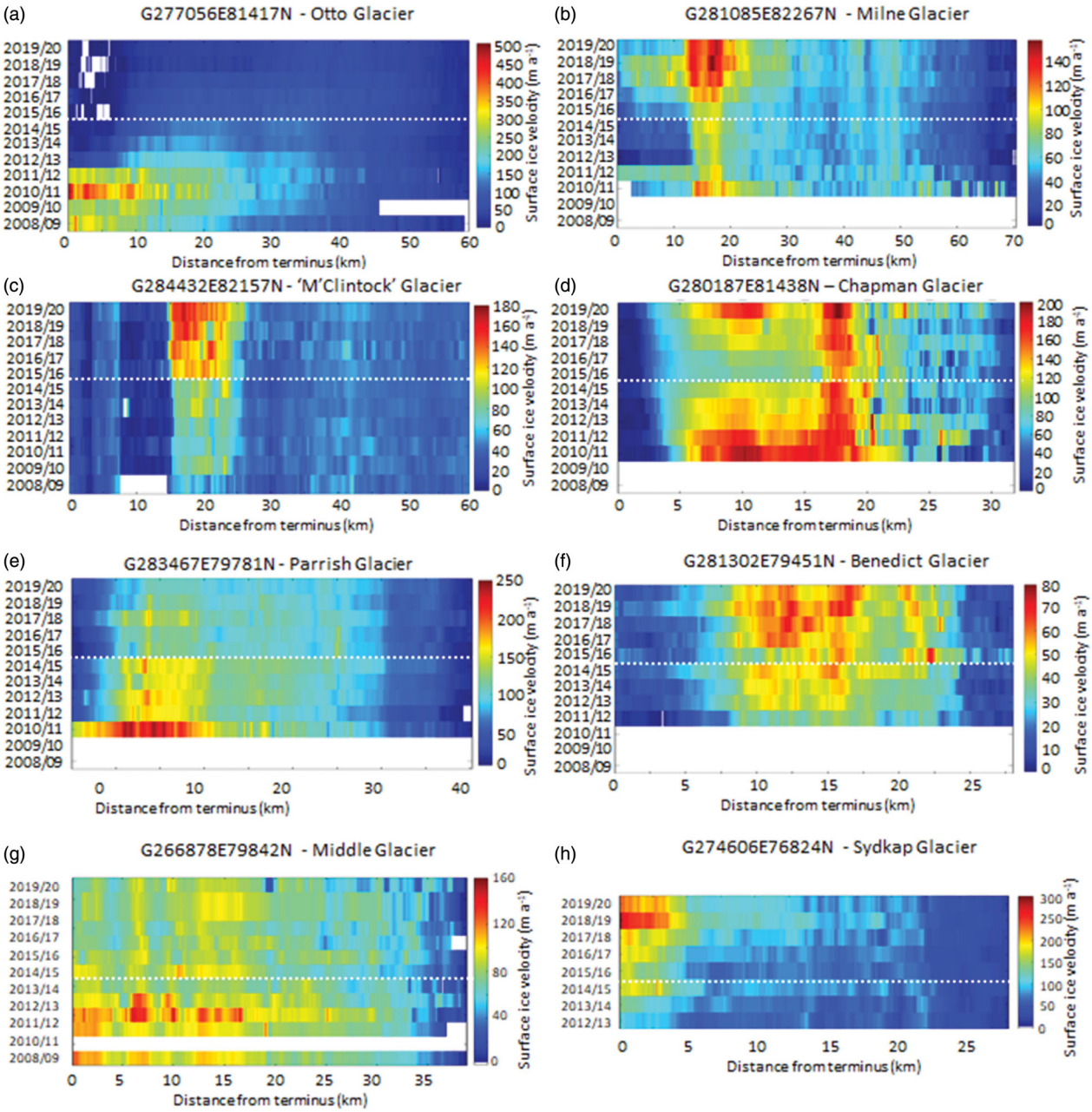

Figure 2. Variations in surface ice velocities over the Radarsat-2 observation period for: (a–d) glaciers located on the Northern Ellesmere Icefield (Otto, Milne, M'Clintock, Chapman), (e–f) Agassiz Ice Cap (Parrish and Benedict), (g) Müller Ice Cap (Middle), and (h) Sydkap Ice Cap (Sydkap). GLIMS ID provided for each identified glacier; results provided below white dashed line were derived by Van Wychen et al. (2016).

result, ice thicknesses tend to increase as glaciers enter these narrow valleys, which causes high driving stresses, which might allow for water to be generated at the bed and basal sliding to be initiated (Burgess et al. 2005; Van Wychen et al. 2017). Furthermore, on these large outlet glaciers, surface meltwater that is generated on the surface and transmitted to the bed during the summer months further facilitates basal sliding (Burgess et al. 2005).

In general, marine-terminating outlet glaciers experience the fastest flow at their termini, while land-terminating glaciers typically slow down near their termini. Our QEI-wide velocity fields largely conform with these expected patterns, with higher velocities mainly observed at marine-terminating glacier fronts where speeds of 100–300 m a^{-1} are common. However, not all large marine-terminating glaciers display this pattern. Indeed, on some large

marine-terminating glaciers, such as Mittie Glacier which drains from Manson Icefield (Figure 1c), and Iceberg Glacier on Axel Heiberg Island (Figure 1g), ice is nearly stagnant near their termini. The velocities observed in these instances are a reflection of cyclical dynamic processes, with these glaciers currently shown to be in the quiescent phase of a surge or pulse cycle (Van Wychen et al. 2017). The fastest ice motion observed in the QEI during the entire observation period occurs on Trinity and Wykeham glaciers, which drain from the Prince of Wales Icefield (Figure 1f). These are the only glaciers within the region where ice velocities currently exceed 1 km a^{-1}, and the present observations are consistent with those reported in previous studies (Harcourt et al. 2020; Millan et al. 2017; Sánchez-Gámez and Navarro 2017; Van Wychen et al. 2014, 2016).

Major areas of variability in ice motion within the QEI (winter 2015/2016–2019/2020)

In general, for the vast majority of glaciers in the region, there was little variability in the flow velocities from winter 2015/2016 to 2019/2020. However, 15 glaciers experienced velocity changes beyond the error margins of the method (Figures 2 and 3). The following sections describe the observed variability of these glaciers, broken down by ice mass, and place this variability within the context of previous studies.

Northern Ellesmere Icefield

Otto, Milne, M'Clintock and Chapman glaciers all experienced significant dynamic changes over the observation period (Figure 2a–d). For Otto Glacier (Figure 2a), a continued deceleration occurred along the main trunk of the glacier ~10–30 km from the calving front. Here, ice velocities decreased from 100–150 m a^{-1} in winter 2015/2016 to <50 m a^{-1} in the same area by winter 2019/2020. This pattern of dynamic change is consistent with the past interpretation that Otto Glacier was transitioning into the quiescent phase of a surge cycle. The surge started in ~2000 and peak surface velocities of ~600–700 m a^{-1} in 2007/8 occurred over the lower 5 km of the glacier (Van Wychen et al. 2016). The active surge phase therefore lasted for ~13 years, and the glacier has now completely transitioned to a period of slow flow. Otto Glacier was previously reported by Hattersley-Smith (1964, 1969) to have been surging in 1963 and 1964, with that surge initiating between 1950 and 1959. This suggests a period of ~30–35 years between repeat surges of this ice mass (assuming that surging is cyclical). For both Milne and M'Clintock Glaciers we determined increasing flow speeds over the observation period. For Milne Glacier, measured surface velocities are generally >100 m a^{-1} in the section of the glacier located 12–20 km from the calving front, which is higher than those determined previously (Figure 2b) (aside from perhaps a limited section of elevated surface velocities in the same area in winter 2010/11). Also of particular interest is the high degree of flow variability in the lowermost ~12 km of the glacier, especially when the results determined here are viewed within the context of those provided by Van Wychen et al. (2016). Here, surface velocities steadily increased from a minimum flow speed of ~20 m a^{-1} in winter 2012/13, to 80–100 m a^{-1} in winter 2018/2019 (similar to what was measured in winter 2011/12 just before the flow minimum). Van Wychen et al. (2016) did not identify Milne Glacier as experiencing any significant change in dynamics, but Millan et al. (2017) used a longer time series to show that the glacier generally slowed from the early 2000s to ~2005, and then began to accelerate between ~2005 and 2015 in the lower ~15 km of the terminus region. The results presented here, when combined with previous results (Van Wychen et al. 2016), show the same trend of acceleration identified by Millan et al. (2017) which has continued each winter to 2019/2020 (Figure 2b). Milne Glacier is therefore experiencing an acceleration toward the present day, which is spatially confined to a region located within ~15 km from the calving front.

Jeffries (1984) had suggested that Milne Glacier was surge-type, based on a ~4 km terminus advance between 1959 and 1983 and the presence of looped and distorted moraines on the glacier surface, which indicated non-steady state motion. Copland et al. (2003) also classified Milne Glacier as possibly surge-type based on the presence of looped moraines. However, the velocity profiles of Milne Glacier presented in Figure 2b indicate that variability in fast and slow flow occurs in the lowermost 15–20 km of the glacier and appears to be relatively restricted to that region. We do not observe a significant up-glacier or down-glacier propagation of high velocities beyond this region, suggesting that the driver of this flow variability differs from that traditionally described for surging glaciers. Rather, the variability in flow speed observed here is more similar to the pulse behavior described by Van Wychen et al. (2016, 2017). Van Wychen et al. (2016) described pulse-type glaciers in the CAA as experiencing short-term (2–5) year periods of faster and slower flow restricted to the

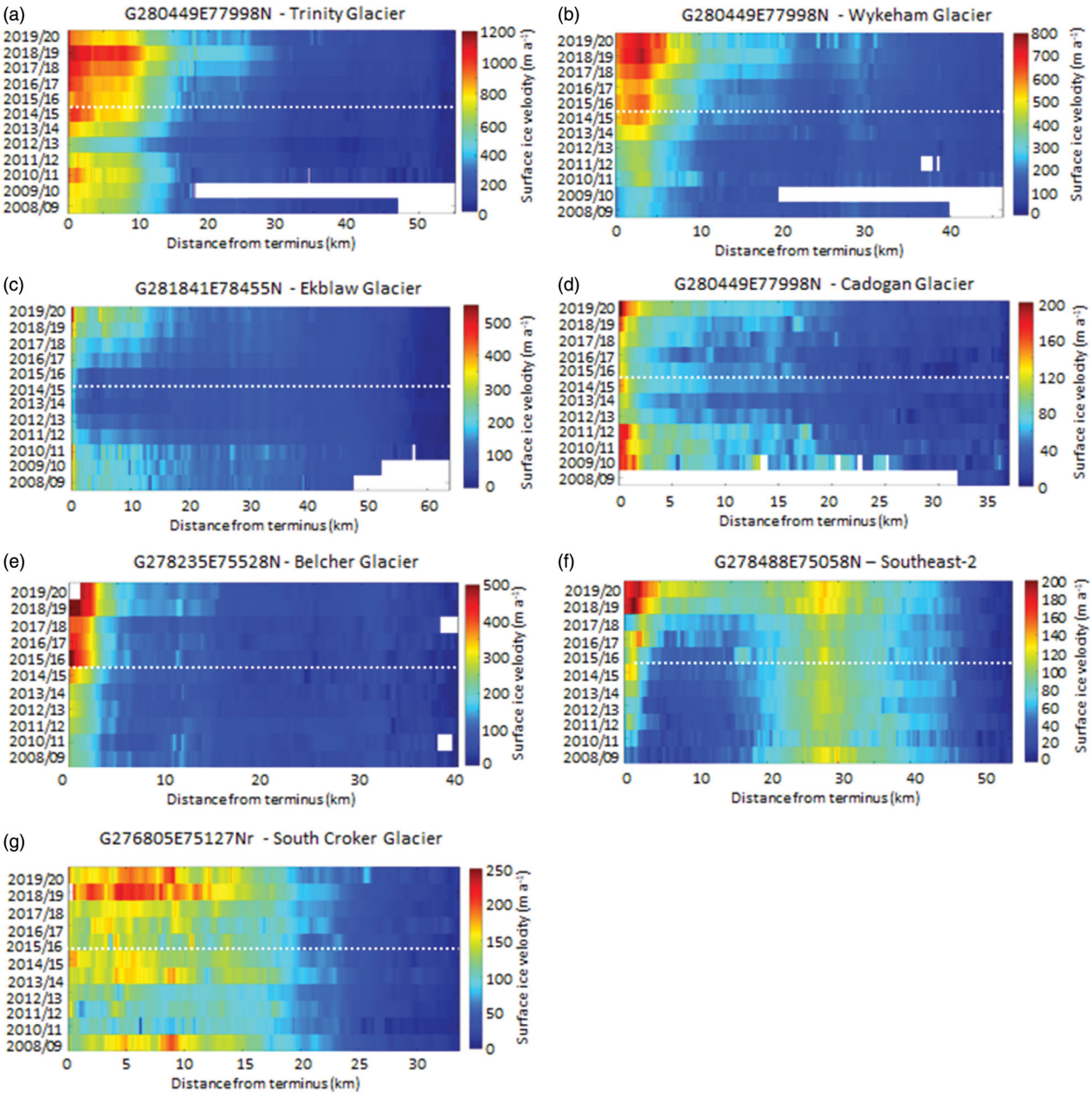

Figure 3. Variations in surface ice velocities over the Radarsat-2 observation period for: (a–d) glaciers located on the Prince of Wales Icefield (Trinity, Wykeham, Ekblaw, Cadogan) and (e–g) glaciers located on Devon Ice Cap (Belcher, Southeast-2, South Croker). Results provided below white dashed line were derived by Van Wychen et al. (2016) in (a-d) and Van Wychen et al. (2017) in (e–g).

lowermost regions of glacier fronts grounded below sea level, potentially coincident with areas containing prominent bedrock features. Given this, we postulate that Milne Glacier is currently in the acceleration phase of a pulse cycle, although more work, preferably including in situ measurements, is necessary in order to better understand the dynamic drivers of this process. Additionally, an assessment of glacier geometry changes associated with the velocity variability observed for Milne Glacier would help further identify the process driving this dynamic change. For example, if surface elevation changes are restricted to only the lowermost terminus regions of the glacier this could provide further evidence of a pulse event that is spatially limited to this part of the glacier (which is distinct from surging, where geometry changes would be expected to occur across most of the glacier length).

There was a general increase in the velocity of M'Clintock Glacier after winter 2015/2016 in the section of the glacier located ~15–25 km from the terminus (Figure 2c). Prior to this time, flow rates were 60–100 m a^{-1} along this section of the glacier, but

they increased to 120–160 m a^{-1} in the subsequent years of observation. Further, the region of accelerating ice motion appears to expand over time, in both up-glacier and down-glacier directions. These velocities are generally higher than what has previously been reported for this ice mass (Millan et al. 2017; Van Wychen et al. 2016). Outside of this section of the glacier, variability in rates of ice flow is negligible. Again, the pattern of dynamic variability is consistent with the pulse mechanism described by Van Wychen et al. (2016), where flow variability is primarily modulated by bedrock topography in lower terminus regions of large outlet glaciers in the QEI, and as such, we attribute the variability observed here to that mechanism. However, more detailed future work is needed to further understand the dynamic processes at play for this glacier.

For Chapman Glacier, Van Wychen et al. (2016) showed a general slowdown of the glacier from winter 2010/2011 to 2014/2015 (Figure 2d). When this record is combined with our continued R2 observations, we report a velocity minimum in the lowermost ~17 km of the glacier in winter 2015/2016. After this time, however, velocities increased through each subsequent winter to 2019/20. The combination of these results show that the glacier undergoes a high degree of velocity variability along the section located from ~5 km to ~20 km from the terminus. Chapman Glacier has previously been identified as surge-type (Copland et al. 2003; Hattersley-Smith 1969), and the results presented here are consistent with that interpretation. The traditional description of surging in the Canadian Arctic is typically of a long quiescent period after a shorter surge phase (Copland et al. 2003), but the results provided here for Chapman Glacier indicate that variations in ice flow in this region can occur in shorter time spans and that more observations are required to further understand the drivers of dynamic change.

Agassiz Ice Cap

For Agassiz Ice Cap, only two glaciers (Parrish and Benedict) displayed significant variations in ice flow rates over the observation period. Parrish Glacier (Figure 2e) exhibited a subtle slowing, which becomes more apparent when compared with the velocities derived for the period prior to winter 2015/2016 (Van Wychen et al. 2016). In this case, the continued slowdown appears to be related to the gradual termination of a pulse cycle originally identified by Van Wychen et al. (2016).

On Benedict Glacier (Figure 2f - termed 'Sawyer Bay Glacier' by Van Wychen et al. (2016) and Williamson et al. (2008)), the ice velocities generally increased between winter 2015/2016 and 2019/2020 along the section of the glacier ~7.5 km to ~17.5 km from the calving front. For example, in 2015/2016, surface ice velocities were ~20–40 m a^{-1} in this region of the glacier, but they increased to speeds of >50 m a^{-1} in subsequent years. Copland et al. (2003) identified Benedict Glacier as a possible surge-type glacier, and the results here indicate that this is likely the case and that the glacier is currently transitioning into a more active phase. None of the other major outlet glaciers on Agassiz Ice Cap displayed any significant variability in ice flow over the observation period.

Müller and Steacie Ice Caps

The surface velocities of Middle Glacier, Müller Ice Cap (Figure 2g), have been generally similar in each winter since 2015/2016, with speeds of 50–100 m a^{-1} along much of the lower 35 km of the glacier trunk. However, it is notable that the velocities determined here are generally lower than those previously reported. In particular, surface velocities of >100 m a^{-1} occurred over the lower 15 km of the glacier in winters 2008/2009, 2010/2011 and 2011/2012 (Figure 2g). Middle Glacier has previously been confirmed as a surge-type glacier (Copland et al. 2003) and our results indicate that the glacier is likely continuing to slow from an active surge in the mid-2000s (Van Wychen et al. 2016). Indeed, these results indicate that the oscillation in flow speeds of Middle Glacier (i.e., the transition into quiescence) occurs over time periods of a decade or more.

The changes at Middle Glacier are somewhat similar to the variability of Good Friday Bay Glacier, Steacie Ice Cap, recently reported by Medrzycka et al. (2019). Good Friday Glacier has undergone ~70 years of terminus advance since 1948, although the velocities there have generally decreased along the length of the glacier since the late 1980s. Medrzycka et al. (2019) attributed this to either a delayed response to the mass balance conditions of the Little Ice Age, or some other type of dynamic instability. We do not further report on the dynamics of Good Friday Bay Glacier given the recent results of Medrzycka et al. (2019) (in part derived from the R2 record described here). Iceberg Glacier is the only other major tidewater terminating glacier draining from the Müller Ice Cap, and our results indicate that it was stagnant (i.e., ice flow rates <20 m a^{-1}) in each winter for which we have observations.

Sydkap Ice Cap

Among the glaciers draining from Sydkap Ice Cap, only the largest outlet, Sydkap Glacier (Figure 2h) exhibited significant flow variability. Suitable R2 imagery to derive ice velocities only started being acquired for Sydkap Ice Cap in winter 2012/2013. As a result, Van Wychen et al. (2016) could only present a short record concerning its variability. However, the results presented here, combined with these earlier results, now provide a record of ice motion for each of the last eight winters, and indicate that the lowermost 5 km of the glacier sped-up over this period. Of particular interest is that in winters 2018/2019 and 2019/2020 ice surface velocities in the near terminus region were >200 m a^{-1}, the highest ever derived for this glacier. Additionally, elevated rates of ice flow are propagating further up-glacier over time. For example, in the winters of 2016/2017 and earlier, ice velocities were generally between 50 and 100 m a^{-1} in the section of the glacier located 5–12 km from the calving front. However, in the winters of 2018/2019 and 2019/2020 ice velocities were generally >100 m a^{-1} in the same region. These results indicate that not only is the lowermost terminus section of the glacier accelerating, but that this acceleration is activating faster ice motion over a relatively broad length of the glacier.

Variability in the flow of Sydkap Glacier has previously been inferred from the identification of an extensively folded glacier surface and terminus retreat of ~9.5 km in the ~1950s (Copland et al. 2003). Copland et al. (2003) attributed this variability to either oscillations due to the tidewater glacier cycle or, more likely they deemed, to surging. The velocity record presented here shows that faster ice motion initiated in the lowermost regions of Sydkap Glacier and that faster ice motion has propagated further up-glacier in each subsequent year of our observations (Figure 2h). This pattern of dynamic change is reminiscent of that reported by Van Wychen et al. (2016) for Trinity and Wykeham Glaciers, which was attributed to 'consistent acceleration' driven by changes in either oceanic or atmospheric conditions. We believe that either a climate-driven consistent acceleration mechanism, or a tidewater glacier cycle, is the more likely cause of the dynamic variability observed for Sydkap Glacier. This is because the recent speed-up has been accompanied by long-term retreat of the glacier front (Cook et al. 2019), whereas we would traditionally expect terminus advance during the acceleration phase of a surge. However, this does not preclude the fact that the current variability could be driven by surging, and highlights the need for further in situ measurements and process-based study of Sydkap Glacier in order to understand the processes driving this acceleration.

Prince of Wales Icefield

Four glaciers on Prince of Wales Icefield displayed significant velocity variability over the observation period: Trinity, Wykeham, Ekblaw and Cadogan (Figure 3a–d, respectively). Beginning with Trinity Glacier, the largest and fastest flowing glacier in the Canadian Arctic, there was a general increase in flow speeds over the observation period, although the highest velocities were observed in winter 2018/2019 rather than 2019/2020 (Figure 3a). In all years, surface velocities were ~800 m a^{-1} or greater in the lowermost 10 km of the glacier. This is a departure from winter velocities previously reported by Van Wychen et al. (2016) where ice motion in this region was mainly between ~600 m a^{-1} and 800 m a^{-1} (results below dashed white line in Figure 3a). These rates are similar to, but higher than, those reported by other studies which utilize independent datasets for the same time periods (Harcourt et al. 2020; Millan et al. 2017; Sánchez-Gámez and Navarro 2017). Of particular interest for Trinity Glacier is the increase in flow speeds in the section of the glacier ~18–30 km from the calving front, which is especially evident in the winter of 2018/2019 when velocities were >400 m a^{-1} along nearly this entire section of the glacier. This pattern is distinct from other years, and indicates that faster ice motion may be expanding upstream to regions of the glacier where it had not previously occurred. Van Wychen et al. (2016) noted that the Trinity Glacier trunk was thinning, and Harcourt et al. (2020) confirmed this and found that the rate of thinning had increased over time. This, combined with the fact that the glacier is grounded below sea level for ~40 km up-glacier from the terminus, caused Harcourt et al. (2020) and Van Wychen et al. (2016) to conclude the glacier was undergoing dynamic thinning and likely susceptible to further thinning, retreat and ultimately greater speed-up. The continued acceleration of the glacier observed here, together with the up-glacier migration of higher velocities, is consistent with that interpretation.

Wykeham Glacier displayed a similar behavior to Trinity, with relatively continuous acceleration of the lower portion of the glacier over the last five years (Figure 3b). Here, surface velocities were between ~500 m a^{-1} and ~600 m a^{-1} in the 5 km sector nearest the calving front in winter 2015/2016, increasing to between ~700 m a^{-1} and ~800 m a^{-1} by winter

2019/2020. The region of higher velocities has also moved up-glacier over time, with a recent speed-up of the section between 10 km and 20 km from the terminus. In this area, velocities increased from ~100 m a^{-1} in 2015/16 to ~300 m a^{-1} by 2018/19 (Figure 3b). When these patterns are combined with earlier results (Van Wychen et al. 2016, results below the white dashed line in Figure 3b) there is a clear speed-up of the glacier over the duration of the R2 velocity record since 2008. Indeed, the results presented here indicate that the 'consistent acceleration' of Wykeham Glacier originally reported by Van Wychen et al. (2016) continues, and that, in addition to this, enhanced velocities now extend up to ~25 km up-glacier from the calving front.

Overall, the results reported here for Wykeham Glacier are consistent with those reported by other studies in years of overlapping data (Harcourt et al. 2020; Millan et al. 2017; Sánchez-Gámez and Navarro 2017). However, Millan et al. (2017) did report surface velocities of ~700 m a^{-1} over the lower terminus of Wykeham Glacier in ~2015 (see Figure 2 and Supplementary Figure 4 in Millan et al. 2017), but we did not observe similar velocities until winters 2018/2019 and 2019/2020 (although the regions of relatively fast and slow flow along the glacier centerline were very similar in both studies). This discrepancy likely arises from the fact that Millan et al. (2017) calculated surface velocities for Wykeham Glacier from feature tracking of approximately annually separated Landsat-7, Landsat 8 and ASTER optical imagery typically collected in summer, while we only used imagery collected during the winter. The Millan et al. (2017) velocities therefore better represent annual velocities which include expected speed-ups during the summer months due to basal lubrication, while our results represent ice motion at times of the year when enhanced basal sliding is unlikely to occur. However, current 'winter-only' velocities of Wykeham Glacier are similar to annual velocities that likely included enhanced basal sliding only a few years ago. This suggests that Wykeham Glacier is transitioning into a new winter-flow regime and that basal sliding is likely now occurring throughout the entire year.

Ekblaw Glacier underwent a consistent speed-up over the winters of 2015/2016 to 2019/2020 (Figure 3c). For example, over nearly the entire glacier surface velocities were <50 m a^{-1} in winter 2015/2016, but in recent years there was a "stepwise" acceleration of surface velocities across the lowermost 12 km section of the glacier, with speeds of ~300 m a^{-1} measured over this entire section by winter 2019/2020. When these results are compared with those reported earlier by Van Wychen et al. (2016), we see that an inflection point occurred around 2014/15, with the glacier slowing during the early portion of the R2 observation period after 2008/9, and then speeding up again toward the present day. This pattern is consistent with the pattern reported by Millan et al. (2017) and conforms to the 'pulse-type' classification attributed to this glacier by Van Wychen et al. (2016).

For Cadogan Glacier (Figure 3d) a similar dynamic pattern occurred as for Ekblaw, although measured surface velocities were lower overall. Here, we again observed a general increase in motion in the lower portion of the glacier in each winter from 2015/2016 to 2019/2020, with elevated surface velocities propagating further up-glacier in each consecutive year. When combined with the results of Van Wychen et al. (2016), we see that minimum ice velocities occurred in the winters of 2012/2013 to 2016/2017. Van Wychen et al. (2016) did not observe enough variability in their velocity record to classify Cadogan as experiencing any type of dynamic change. However, the results here indicate that the glacier does undergo multi-annual variations in flow. When these results are combined with those described by Millan et al. (2017) for Cadogan in the early-1990s (see supplementary Figure 4 of that work), there is further evidence to support this interpretation.

Devon Ice Cap

For Devon Ice Cap, the recent speed-ups of Belcher and Southeast-2 glaciers are notable. For Belcher Glacier (Figure 3e), surface velocities in the lower terminus region (e.g., within 5 km of the calving front) were mainly >400 m a^{-1} during all winters since 2015/2016. This is a significant acceleration from previously reported values, where motion mainly ranged between 250 m a^{-1} and 350 m a^{-1} (Burgess et al. 2005; Millan et al. 2017; Van Wychen et al. 2012, 2017). Additionally, in the two most recent years of observation (winters 2018/2019 and 2019/2020), surface velocities were between 450–550 m a^{-1} in the lowermost terminus region. These velocities are similar to the peak summer velocities determined from dGPS observations in a similar location by Danielson and Sharp (2013), which were correlated with timing of the drainage of surface meltwater ponds. In addition, the elevated surface velocities, as compared to all other years presented, occurred over the lowermost ~10–14 km of the glacier. Up-glacier of this location surface flow speeds in all years varied little.

Van Wychen et al. (2017) speculated that Belcher Glacier was experiencing 'consistent acceleration', distinct from cyclical surge or pulse processes and similar to the dynamic instability reported for Trinity and Wykeham glaciers by Van Wychen et al. (2016). The results reported here confirm the assertion that Belcher Glacier is undergoing a change in its dynamic behavior, which has been manifested as further acceleration of its terminus region. Given the widespread acceleration determined in the most recent years of observation, the glacier may become less stable and more prone to speed-up in the future, especially given the fact that much of the main trunk of the glacier (from the terminus to ~20 km up-glacier) is grounded below sea level (Dowdeswell et al. 2004).

For Southeast-2 Glacier (Figure 3f), there was a general increase in surface velocities from winter 2015/2016 to 2019/2020. In particular, in the last two winters of observation, the lowermost 5 km section of the glacier accelerated to speeds of 160–200 m a^{-1}. There has also been an approximate doubling in flow speeds between 5 km and 25 km from the terminus, increasing from ~20–60 m a^{-1} in 2015/2016 to ~80–120 m a^{-1} by 2019/2020. Burgess et al. (2005) and Van Wychen et al. (2012) both inferred that the glacier was surge-type. The observations presented here confirm that inference, and suggest that the glacier could be transitioning into an active surge phase.

Finally, the South Croker Bay Glacier (Figure 3g), has generally increased in flow speed since winter 2015/2016, with the highest measured velocities of >200 m a^{-1} in the lowermost 12 km of the glacier observed in winter 2018/2019. However, over the entire R2 era since 2008/9 it is clear that this glacier undergoes considerable inter-annual variability in surface velocity, consistent with the findings of Van Wychen et al. (2017).

Causes of observed variability

For the majority of the glaciers with significant velocity variability (all but Trinity, Wykeham, and Belcher), the variations are consistent with cyclical processes (e.g., pulse- or surge-type glaciers). The dynamic record presented here indicates that ice flow in the Canadian High Arctic varies on multiple timescales, sometimes oscillating between periods of slower and faster flow over approximately decadal timeframes (e.g., Ekblaw Glacier, Figure 3c). This pattern is in contrast to the traditional description of surging within this region, where active periods of accelerated ice flow last for ~5–10+ years, followed by decades of slow, quiescent flow (Copland et al. 2003). Our results show that although this is true for some glaciers (e.g., Otto), it certainly is not true for all glaciers within the region (e.g., Chapman). Indeed, these results provide further evidence that conceptual models of surging and pulsing need to be more inclusive of a wide range of dynamic behaviors and timescales of oscillation. Furthermore, these results and interpretations provide further evidence of the importance of long-term dynamic monitoring programs in order to better quantify and characterize a broad range of glacier behaviors.

Of considerable note is the continued acceleration of Trinity, Wykeham and Belcher glaciers over the past decade. For Trinity, Wykeham and Belcher, the acceleration of these glaciers has already been attributed to dynamic thinning (Van Wychen et al. (2016, 2017); Harcourt et al. (2020)), driven by changing ocean and/or atmospheric conditions. Cook et al. (2019) reported that each of these glaciers has been experiencing retreat of the calving front. This is of considerable importance given that these are some of the fastest flowing glaciers within the Canadian Arctic, and major sources of mass loss to the ocean (discussed more in the following section). Of particular importance is the finding that winter flow rates for these glaciers are similar to peak summer flow velocities determined just a few years prior, suggesting a shift with regard to the flow regime, where glaciers might be becoming ungrounded at their fronts, which warrants further investigation.

To better determine the drivers of the observed dynamic variability, further work and process-based studies which integrate field observations (e.g., ground-penetrating radar surveys) and additional remote sensing datasets (e.g., DEMs, melt mapping and greater density of surface velocity measurements) are needed. This is beyond the scope of this study, which focuses on reporting, quantifying and characterizing the observed velocity variability over the last 5 winters and assessing how it has changed since the start of the R2 era in 2008.

Ice flux to the ocean

Table 2 provides the calculated ice flux to the ocean for each winter from 2015/2016 to 2019/2020, broken down by glacier and ice mass. Total dynamic discharge for the QEI over the observation period ranged from a minimum of 2.369 ± 0.475 Gt a^{-1} in 2015/2016 to a maximum of 3.203 ± 0.554 Gt a^{-1} in winter 2019/2020, with a mean of 2.775 ± 0.516 Gt a-1 (Table 2).

Table 2a. Calculated winter ice flux to the ocean for the main marine-terminating ice masses of the Queen Elizabeth Islands, 2015/2016 to 2017/2018.

					Winter ice flux (Gt a^{-1})		
Ice mass	Glacier name	GLIMS ID	Lat	Long	2015/2016	2016/2017	2017/2018
Northern Ellesmere							
	Otto	G277056E81417N	81.30	−84.70	0.002 ± 0.002	0.006 ± 0.003	0.002 ± 0.002
	Yelverton	G279683E81662N	81.88	−79.53	0.054 ± 0.009	0.065 ± 0.010	0.069 ± 0.011
	Yelverton Inlet South	G282159E81936N	82.01	−79.60	0.002 ± 0.002	0.003 ± 0.003	0.002 ± 0.002
	Yelverton Inlet East	G281287E82135N	82.14	−80.75	0.009 ± 0.003	0.012 ± 0.004	0.007 ± 0.003
		G279030E82222N	82.24	−81.72	0.002 ± 0.002	0.003 ± 0.002	0.003 ± 0.002
		G278514E82357N	82.42	−82.54	0.009 ± 0.006	0.013 ± 0.007	0.022 ± 0.009
	Milne	G281085E82267N	82.52	−80.69	0.008 ± 0.003	0.011 ± 0.003	0.013 ± 0.004
	M'Clintock	G284432E82157N	82.52	−76.01	0.005 ± 0.002	0.002 ± 0.007	0.002 ± 0.008
	Disraeli	G287533E82397N	82.69	−72.53	0.010 ± 0.003	0.013 ± 0.003	0.014 ± 0.004
		G289487E82706N	82.84	−70.87	0.014 ± 0.005	0.014 ± 0.005	0.015 ± 0.006
Total Northern Ellesmere discharge					0.115 ± 0.037	0.142 ± 0.047	0.149 ± 0.051
Agassiz ice cap							
	Lake Tuborg	G285207E80719N	80.89	−76.14	0.021 ± 0.003	0.024 ± 0.004	0.023 ± 0.003
	Antoinette	G284641E80537N	80.81	−76.34	0.004 ± 0.003	0.003 ± 0.003	0.004 ± 0.003
	d'Iberville	G283470E80355N	80.56	−77.92	0.007 ± 0.003	0.007 ± 0.003	0.007 ± 0.003
	Cañon	G281517E79944N	79.68	−79.65	0.056 ± 0.010	0.060 ± 0.011	0.063 ± 0.011
	Benedict	G281302E79451N	79.37	−78.01	0.007 ± 0.004	0.008 ± 0.004	0.011 ± 0.004
	Parrish	G283467E79781N	79.57	−77.19	0.004 ± 0.003	0.004 ± 0.003	0.007 ± 0.004
		G284116E79986N	79.82	−74.93	0.003 ± 0.003	0.003 ± 0.003	0.003 ± 0.003
	John Richardson Bay South	G286085E80203N	80.07	−72.39	0.014 ± 0.004	0.012 ± 0.004	0.013 ± 0.004
		G286421E80454N	80.23	−72.44	0.004 ± 0.003	0.003 ± 0.002	0.003 ± 0.002
		G287628E80586N	80.56	−70.82	0.003 ± 0.001	0.003 ± 0.001	0.003 ± 0.001
Total Agassiz ice cap discharge					0.123 ± 0.037	0.127 ± 0.087	0.137 ± 0.038
Steacie and Müller ice caps							
	Iceberg	G267715E79629N	79.43	−92.38	0.006 ± 0.003	0.006 ± 0.003	0.006 ± 0.003
	Good Friday Bay	G268921E78794N	78.55	−91.77	0.041 ± 0.008	0.036 ± 0.008	0.039 ± 0.008
Total Steacie and Müller ice caps discharge					0.047 ± 0.011	0.042 ± 0.011	0.045 ± 0.011
Prince of Wales Icefield							
		G279474E77543N	77.39	−80.99	0.003 ± 0.002	0.004 ± 0.002	0.005 ± 0.002
		G279772E77453N	77.31	−80.30	0.002 ± 0.001	0.002 ± 0.001	0.002 ± 0.001
		G280219E77500N	77.32	−79.62	0.025 ± 0.005	0.042 ± 0.007	0.042 ± 0.007
		G280779E77365N	77.32	−79.05	0.001 ± 0.001	0.002 ± 0.001	0.002 ± 0.001
		G281018E77375N	77.37	−78.93	0.000 ± 0.000	0.000 ± 0.000	0.000 ± 0.000
		G281001E77406N	77.39	−78.90	0.001 ± 0.001	0.001 ± 0.001	0.001 ± 0.001
		G281252E77458N	77.41	−78.75	0.015 ± 0.005	0.015 ± 0.005	0.014 ± 0.005
		G280783E77677N	77.59	−78.07	0.046 ± 0.037	0.056 ± 0.039	0.041 ± 0.034
		G281497E77785N	77.78	−78.09	0.028 ± 0.014	0.011 ± 0.011	0.011 ± 0.001
	Wykeham	G280449E77998N	77.90	−78.62	0.413 ± 0.047	0.376 ± 0.044	0.426 ± 0.048
		G280449E77998N	77.88	−78.31	0.010 ± 0.005	0.003 ± 0.003	0.003 ± 0.003
	Trinity	G280449E77998N	77.90	−78.57	0.928 ± 0.095	1.002 ± 0.102	1.067 ± 0.108
		G280449E77998N	77.86	−78.54	0.001 ± 0.001	0.001 ± 0.001	0.001 ± 0.001
		G281761E78078N	78.00	−78.25	0.002 ± 0.002	0.002 ± 0.002	0.001 ± 0.001
		G282272E78063N	77.99	−77.92	0.011 ± 0.003	0.013 ± 0.003	0.013 ± 0.003
		G282649E78046N	77.98	−77.36	0.003 ± 0.002	0.003 ± 0.002	0.002 ± 0.002
	Cadogan	G282399E78249N	78.24	−76.92	0.037 ± 0.012	0.048 ± 0.012	0.047 ± 0.012
		G284750E78374N	78.39	−75.22	0.000 ± 0.000	0.000 ± 0.000	0.000 ± 0.000
		G284476E78348N	78.40	−75.29	0.001 ± 0.001	0.001 ± 0.001	0.001 ± 0.001
		G284414E78401N	78.42	−75.45	0.002 ± 0.002	0.002 ± 0.002	0.002 ± 0.002
	Ekblaw	G281841E78455N	78.51	−76.70	0.076 ± 0.012	0.117 ± 0.015	0.140 ± 0.017
		G284232E78592N	78.53	−75.32	0.010 ± 0.003	0.008 ± 0.003	0.009 ± 0.003
	Alfred Newton	G284659E78590N	78.57	−74.89	0.009 ± 0.003	0.001 ± 0.001	0.002 ± 0.002
	Leffert	G282971E78675N	78.69	−74.92	0.011 ± 0.003	0.010 ± 0.003	0.013 ± 0.004
	Stygge	G281886E78657N	78.77	−78.24	0.009 ± 0.003	0.011 ± 0.004	0.012 ± 0.004
		G280794E78802N	78.85	−78.20	0.009 ± 0.002	0.009 ± 0.002	0.010 ± 0.002
		G281386E78908N	78.95	−77.99	0.006 ± 0.002	0.008 ± 0.002	0.006 ± 0.002
Total Prince of Wales Icefield discharge					1.659 ± 0.264	1.748 ± 0.269	1.873 ± 0.267
Sydkap ice cap							
	Sydkap	G274606E76824N	76.66	−85.27	0.003 ± 0.006	0.037 ± 0.006	0.039 ± 0.006
Total Sydkap ice cap discharge					0.003 ± 0.006	0.037 ± 0.006	0.039 ± 0.006
Manson Icefield							
	Mittie	G279922E76831N	76.87	−79.34	0.031 ± 0.025	0.020 ± 0.020	0.036 ± 0.027

(*Continued*)

Table 2a. Continued.

Ice mass	Glacier name	GLIMS ID	Lat	Long	Winter ice flux (Gt a^{-1}) 2015/2016	2016/2017	2017/2018
Total Manson Icefield discharge					0.031 ± 0.025	0.020 ± 0.020	0.036 ± 0.027
Devon ice cap							
	Sverdrup	G276838E75498N	75.72	−83.19	0.008 ± 0.005	0.008 ± 0.005	0.007 ± 0.004
	Eastern	G277553E75571N	75.80	−81.99	0.017 ± 0.004	0.018 ± 0.004	0.012 ± 0.003
	Belcher (South Arm)	G278235E75528N	75.67	−81.33	0.163 ± 0.021	0.151 ± 0.019	0.147 ± 0.019
	Belcher (North Arm)	G278235E75528N	75.70	−81.30	0.005 ± 0.003	0.004 ± 0.003	0.006 ± 0.003
	Fitzroy (South Arm)	G279123E75409N	75.45	−80.47	0.042 ± 0.006	0.039 ± 0.006	0.033 ± 0.006
	Fitzroy (North Arm)	G279123E75409N	75.47	−80.51	0.002 ± 0.002	0.002 ± 0.002	0.004 ± 0.002
	East-5	G279852E75328N	75.30	−79.82	0.009 ± 0.005	0.005 ± 0.004	0.004 ± 0.004
	East-6	G279403E75242N	75.17	−79.99	0.003 ± 0.002	0.002 ± 0.002	0.002 ± 0.002
	Southeast-1/2		74.98	−80.41	0.064 ± 0.018	0.093 ± 0.022	0.094 ± 0.022
	East-7	G278488E75058N	75.06	−80.40	0.010 ± 0.004	0.009 ± 0.004	0.008 ± 0.004
	Southeast-3	G279279E74787N	74.80	−80.37	0.011 ± 0.011	0.019 ± 0.013	0.018 ± 0.013
	South Croker Bay		74.84	−83.18	0.048 ± 0.009	0.052 ± 0.009	0.050 ± 0.009
	North Croker Bay	G276805E75127N	74.91	−83.62	0.009 ± 0.005	0.009 ± 0.005	0.014 ± 0.006
Total discharge for Devon ice cap					0.391 ± 0.095	0.411 ± 0.098	0.399 ± 0.097
Total QEI discharge to the ocean					2.369 ± 0.475	2.541 ± 0.493	2.680 ± 0.509

Table 2b. Calculated winter ice flux to the ocean for the main marine-terminating ice masses of the Queen Elizabeth Islands, 2018/2019 to 2019/2020.

Ice mass	Glacier name	GLIMS ID	Lat	Long	Winter ice flux (Gt a^{-1}) 2018/2019	2019/2020
Northern Ellesmere						
	Otto	G277056E81417N	81.30	−84.70	0.003 ± 0.003	0.003 ± 0.003
	Yelverton	G279683E81662N	81.88	−79.53	0.078 ± 0.012	0.053 ± 0.009
	Yelverton Inlet South	G282159E81936N	82.01	−79.60	0.002 ± 0.002	0.002 ± 0.002
	Yelverton Inlet East	G281287E82135N	82.14	−80.75	0.010 ± 0.004	0.009 ± 0.003
		G279030E82222N	82.24	−81.72	0.005 ± 0.003	0.003 ± 0.002
		G278514E82357N	82.42	−82.54	0.014 ± 0.007	0.014 ± 0.007
	Milne	G281085E82267N	82.52	−80.69	0.014 ± 0.004	0.010 ± 0.003
	M'Clintock	G284432E82157N	82.52	−76.01	0.003 ± 0.009	0.011 ± 0.004
	Disraeli	G287533E82397N	82.69	−72.53	0.017 ± 0.004	0.004 ± 0.002
		G289487E82706N	82.84	−70.87	0.016 ± 0.006	0.016 ± 0.006
Total Northern Ellesmere discharge					0.162 ± 0.054	0.125 ± 0.041
Agassiz ice cap						
	Lake Tuborg	G285207E80719N	80.89	−76.14	0.030 ± 0.004	0.023 ± 0.003
	Antoinette	G284641E80537N	80.81	−76.34	0.004 ± 0.003	0.003 ± 0.003
	d'Iberville	G283470E80355N	80.56	−77.92	0.007 ± 0.003	0.005 ± 0.003
	Cañon	G281517E79944N	79.68	−79.65	0.072 ± 0.012	0.065 ± 0.001
	Benedict	G281302E79451N	79.37	−78.01	0.013 ± 0.005	0.009 ± 0.004
	Parrish	G283467E79781N	79.57	−77.19	0.007 ± 0.004	0.011 ± 0.004
		G284116E79986N	79.82	−74.93	0.003 ± 0.003	0.003 ± 0.003
	John Richardson Bay South	G286085E80203N	80.07	−72.39	0.013 ± 0.004	0.013 ± 0.004
		G286421E80454N	80.23	−72.44	0.004 ± 0.003	0.003 ± 0.002
		G287628E80586N	80.56	−70.82	0.003 ± 0.001	0.000 ± 0.000
Total Agassiz ice cap discharge					0.156 ± 0.042	0.135 ± 0.027
Steacie and Müller ice caps						
	Iceberg	G267715E79629N	79.43	−92.38	0.004 ± 0.003	0.004 ± 0.003
	Good Friday Bay	G268921E78794N	78.55	−91.77	0.039 ± 0.008	0.034 ± 0.008
Total Steacie and Müller ice caps discharge					0.043 ± 0.011	0.038 ± 0.011
Prince of Wales Icefield						
		G279474E77543N	77.39	−80.99	0.006 ± 0.002	0.010 ± 0.003
		G279772E77453N	77.31	−80.30	0.001 ± 0.001	0.001 ± 0.001
		G280219E77500N	77.32	−79.62	0.060 ± 0.008	0.071 ± 0.009
		G280779E77365N	77.32	−79.05	0.002 ± 0.001	0.002 ± 0.001
		G281018E77375N	77.37	−78.93	0.000 ± 0.000	0.000 ± 0.001
		G281001E77406N	77.39	−78.90	0.001 ± 0.001	0.001 ± 0.001
		G281252E77458N	77.41	−78.75	0.016 ± 0.005	0.015 ± 0.005
		G280783E77677N	77.59	−78.07	0.047 ± 0.036	0.083 ± 0.039
		G281497E77785N	77.78	−78.09	0.013 ± 0.012	0.106 ± 0.024
	Wykeham	G280449E77998N	77.90	−78.62	0.519 ± 0.057	0.501 ± 0.056
		G280449E77998N	77.88	−78.31	0.003 ± 0.003	0.006 ± 0.004
	Trinity	G280449E77998N	77.90	−78.57	1.140 ± 0.115	1.091 ± 0.111
		G280449E77998N	77.86	−78.54	0.002 ± 0.001	0.004 ± 0.002
		G281761E78078N	78.00	−78.25	0.001 ± 0.001	0.004 ± 0.002
		G282272E78063N	77.99	−77.92	0.014 ± 0.003	0.017 ± 0.003
		G282649E78046N	77.98	−77.36	0.002 ± 0.002	0.002 ± 0.002

(*Continued*)

Table 2b. Continued.

Ice mass	Glacier name	GLIMS ID	Lat	Long	Winter ice flux (Gt a^{-1}) 2018/2019	Winter ice flux (Gt a^{-1}) 2019/2020
	Cadogan	G282399E78249N	78.24	−76.92	0.068 ± 0.015	0.067 ± 0.015
		G284750E78374N	78.39	−75.22	0.000 ± 0.000	0.000 ± 0.000
		G284476E78348N	78.40	−75.29	0.003 ± 0.001	0.001 ± 0.001
		G284414E78401N	78.42	−75.45	0.002 ± 0.002	0.004 ± 0.002
	Ekblaw	G281841E78455N	78.51	−76.70	0.166 ± 0.019	0.186 ± 0.021
		G284232E78592N	78.53	−75.32	0.009 ± 0.003	0.008 ± 0.002
	Alfred Newton	G284659E78590N	78.57	−74.89	0.001 ± 0.001	0.001 ± 0.001
	Leffert	G282971E78675N	78.69	−74.92	0.011 ± 0.004	0.011 ± 0.004
	Stygge	G281886E78657N	78.77	−78.24	0.014 ± 0.004	0.011 ± 0.004
		G280794E78802N	78.85	−78.20	0.012 ± 0.002	0.014 ± 0.003
		G281386E78908N	78.95	−77.99	0.007 ± 0.002	0.007 ± 0.002
Total Prince of Wales Icefield discharge					2.120 ± 0.301	2.224 ± 0.319
Sydkap ice cap						
	Sydkap	G274606E76824N	76.66	−85.27	0.057 ± 0.008	0.042 ± 0.007
Total Sydkap ice cap discharge					0.057 ± 0.008	0.042 ± 0.007
Manson Icefield						
	Mittie	G279922E76831N	76.87	−79.34	0.024 ± 0.024	0.023 ± 0.022
Total Manson Icefield discharge					0.024 ± 0.024	0.023 ± 0.022
Devon ice cap						
	Sverdrup	G276838E75498N	75.72	−83.19	0.007 ± 0.004	0.006 ± 0.004
	Eastern	G277553E75571N	75.80	−81.99	0.017 ± 0.004	0.011 ± 0.003
	Belcher (South Arm)	G278235E75528N	75.67	−81.33	0.191 ± 0.023	0.285 ± 0.031
	Belcher (North Arm)	G278235E75528N	75.70	−81.30	0.004 ± 0.003	0.005 ± 0.002
	Fitzroy (South Arm)	G279123E75409N	75.45	−80.47	0.044 ± 0.007	0.041 ± 0.006
	Fitzroy (North Arm)	G279123E75409N	75.47	−80.51	0.002 ± 0.002	0.002 ± 0.002
	East-5	G279852E75328N	75.30	−79.82	0.008 ± 0.004	0.006 ± 0.004
	East-6	G279403E75242N	75.17	−79.99	0.002 ± 0.002	0.002 ± 0.002
	Southeast-1/2	G278488E75058N	74.98	−80.41	0.131 ± 0.024	0.155 ± 0.027
	East-7		75.06	−80.40	0.010 ± 0.004	0.012 ± 0.005
	Southeast-3	G279279E74787N	74.80	−80.37	0.014 ± 0.012	0.012 ± 0.012
	South Croker Bay	G276805E75127N	74.84	−83.18	0.074 ± 0.011	0.060 ± 0.010
	North Croker Bay		74.91	−83.62	0.017 ± 0.006	0.016 ± 0.006
Total discharge for Devon ice cap					0.521 ± 0.106	0.613 ± 0.114
Total QEI discharge to the ocean					3.084 ± 0.548	3.203 ± 0.554

Noteworthy is the fact that the mean values have increased in each successive year, although the overall change in discharge is within error margins and we did not take into account ice fluxes from changes in terminus position. Nevertheless, with the consistent increase in ice flux each year, coupled with the acceleration of some of the largest outlet glaciers within the QEI such as Trinity, Wykeham and Belcher, it stands to reason that the amount of ice being lost to the ocean is increasing over time. The results reported here are consistent with those reported previously (Van Wychen et al. 2012, 2014, 2016, 2017), and continue to indicate that mass loss via flux to the ocean is a relatively small component of total glacier mass loss within the region (consistent with Millan et al. 2017; Van Wychen et al. 2014). For example, Ciracì et al. (2020) used Gravity Recovery and Climate Experiment data to determine an average total mass balance of -41.2 ± 7 Gt a^{-1} for the glaciers of the CAA over the period April 2002 to September 2019, meaning that our estimated ice fluxes to the ocean account for ~5.8% and 7.8% of this total. However, our estimates of ice flux to the ocean are generally less (~1 Gt a^{-1} lower) than those reported by Millan et al. (2017) in years of overlapping data, likely because we only used winter-derived surface velocities to calculate discharge.

Figure 4 presents the distribution of ice flux to the ocean for the winter of 2019/2020 and highlights the uneven discharge between individual ice masses and glaciers within the Canadian Arctic. Although Figure 4 only shows the ice flux in winter 2019/2020, the geographical distribution of flux and the importance of individual glaciers presented here is representative of all winters since 2015/2016. The Prince of Wales Icefield is the largest source of ice flux to the ocean in the QEI, responsible for about 70% of the total (Figure 4). Indeed, for the QEI as a whole, the Trinity and Wykeham Glacier complex of the Prince of Wales Icefield continues to be the major conduit of mass loss via dynamic discharge, contributing ~50% of all the ice discharged collectively from Devon, Ellesmere and Axel Heiberg Islands.

Devon Ice Cap is the next largest contributor to mass flux to the ocean from the QEI, responsible for about 20% of total dynamic discharge (Figure 4). This is also the only ice mass of the QEI where observed changes in discharge were beyond error margins from 2015/2016 to 2019/2020, increasing from

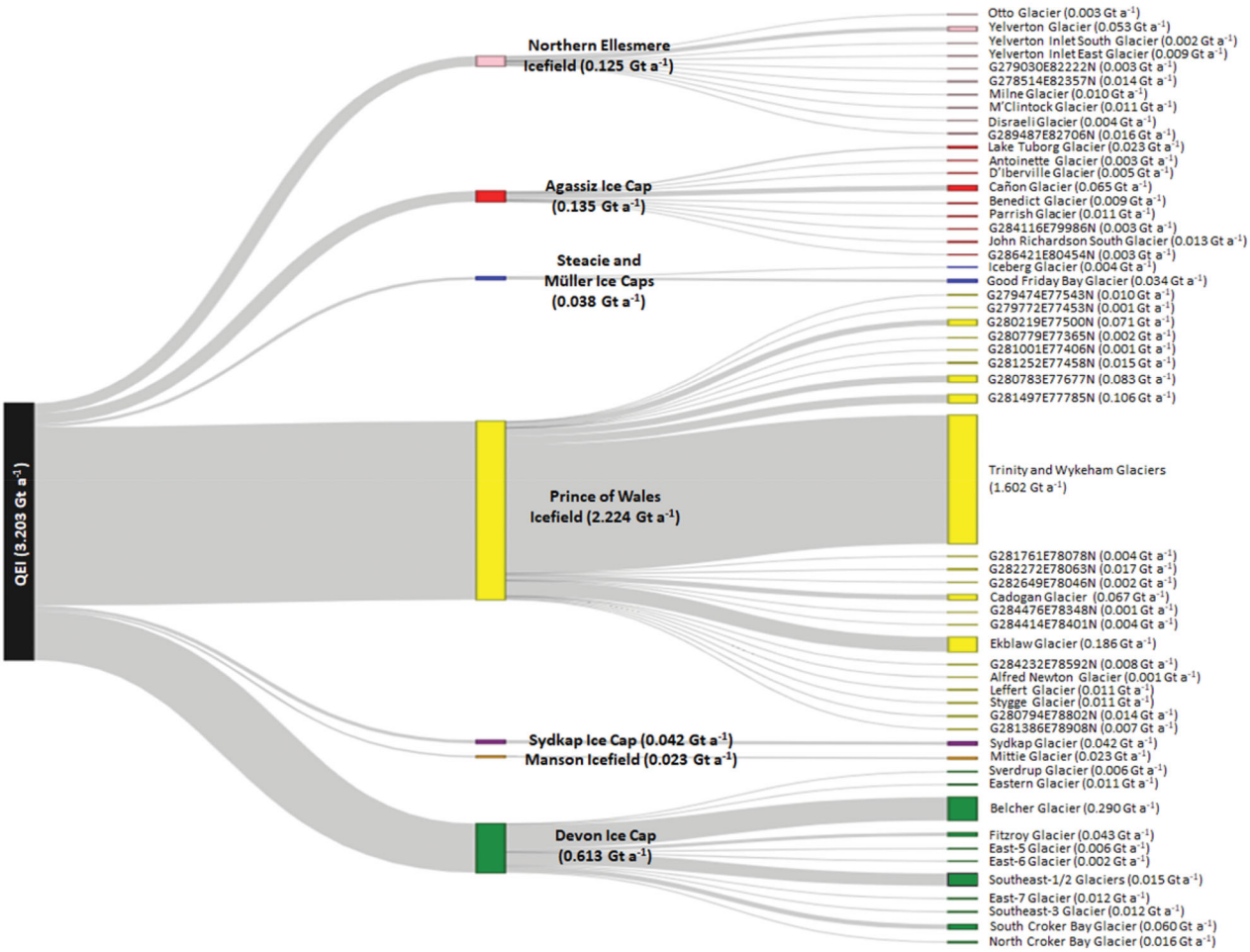

Figure 4. Distribution of ice discharged to the ocean from the ice masses of the Queen Elizabeth Islands, broken down by ice mass and glacier, for winter 2019/2020. GLIMS ID provided for unnamed glaciers.

$\sim 0.391 \pm 0.095$ Gt a^{-1} in winter 2015/16 to $\sim 0.613 \pm 0.114$ Gt a^{-1} in winter 2019/2020 (Table 2). This escalation in ice discharge was primarily driven by the speed-up of Belcher Glacier, and to a lesser degree the speed-up of the Southeast-1/2 basin. Belcher Glacier accounted for ~40% of total ice discharge from Devon Ice Cap in all winters except for 2019/2020, when it accounted for ~50% of total ice discharge. Similarly, for Southeast-1/2, it accounted for ~14% of total ice discharge in 2015/2016 and ~22% of total ice discharge in 2019/2020. These observations confirm previous work, which note that the total dynamic ice discharge of the QEI is sensitive to changes in discharge from just a few major outlet glaciers (Van Wychen et al. 2014, 2016).

Conclusions and outlook

In this study, we presented surface velocities for the ice masses of the Canadian High Arctic derived from R2 imagery collected each winter from 2015/2016 to 2019/2020, and calculated the dynamic discharge to the ocean from every major outlet glacier. When these results are combined with those of previous studies (Harcourt et al. 2020; Millan et al. 2017; Sánchez-Gámez and Navarro 2017; Strozzi et al. 2017; Van Wychen et al. 2016, 2017), they provide a robust record of ice motion within the region for the last ~12 years. For the vast majority of glaciers, we observed little year-to-year variability in winter ice motion within the region, with much of the variability attributable to cyclical dynamic processes. However, Trinity, Wykeham, and Belcher Glaciers have consistently accelerated over the observation period, indicating that previously reported accelerations of these glaciers have continued (Harcourt et al. 2020; Millan et al. 2017; Van Wychen et al. 2016, 2017). Given that these accelerations cannot be explained by surge- or pulse-type processes, it is likely that these glaciers are becoming ungrounded at their termini due to high rates of thinning that have been reported previously (Harcourt et al. 2020; Van Wychen et al. 2016, 2017).

This further suggests that these glaciers are responding to external forces and evolving accordingly. Driven mainly by the accelerations of these glaciers, there was also an increased ice flux to the ocean, from 2.369 ± 0.475 Gt a^{-1} in winter 2015/2016 to 3.203 ± 0.554 Gt a^{-1} in winter 2019/2020. This is of concern given that these glaciers drain into Baffin Bay, and the speed-up and break-up of the Trinity, Wykeham and Belcher Glaciers appears to be resulting in increased iceberg production (Dalton et al. 2019), which may increase hazards to shipping operating in this region.

These results have provided unprecedented temporal and spatial detail for characterizing glacier motion, and its variability, in the QEI during this time and have provided some of the first regional estimates of ice flux to the ocean. Indeed, the derived velocities showcase how powerful a tool the R2 sensor has been for glacier velocity mapping, and as the RCM becomes the next major SAR sensor that will be utilized to measure glacier motion across Canada, these records provide an important baseline against which future change can be compared. Although speckle tracking of R2 imagery provided a robust methodology to determine glacier motion at regional scales in the Canadian Arctic, the more rapid orbital repeat of the RCM (4 days for RCM as opposed to 24 days for R2) means that a combined InSAR and speckle tracking methodology (similar to Sánchez-Gámez and Navarro (2017)) might be an appropriate approach in the future.

Our work here exclusively utilized winter imagery in order to identify and detail multi-annual variability in glacier motion, which provided a record of the velocity and discharge fluctuations of surge-type and pulse-type glaciers within the QEI. Despite being a winter-only record, these results are useful for identifying glaciers with significant variability in ice motion on which more in-depth process-based studies should be undertaken. These studies should include summer-derived velocities, when these glaciers are typically more active, and investigate the links between glacier velocity variability and sea ice buttressing at the individual glacier scale (rather than the regional approach taken here). However, this is beyond the scope of this study, where our goal has been to use the winter record of ice motion to characterize how background ice motion has evolved over the last decade and update dynamic ice discharge estimates to the ocean.

There continues to be significant utility in revisiting and exploiting the remainder of the R2 image catalogue to create an even denser record of glacier motion within Canada. This includes the derivation of glacier velocities from all suitable acquisitions of R2 data. Future work should focus on harvesting these records to explore the seasonality of glacier flow within the region, which is currently understudied. Additionally, the derived R2 velocity record should be combined with recently released records of optically derived ice motion (e.g., GoLIVE), as well as records of glacier surface elevations (e.g., ArcticDEM), to better understand fluctuations in glacier geometry within the region. As such, the fusion of these datasets will provide significant information for future process-based studies that will further our understanding of dynamic glacier processes within the Canadian Arctic.

Funding

We gratefully acknowledge support to carry out this work from the ArcticNet Network of Centres of Excellence ('GO-Ice project' support to WVW and LC), Environment and Climate Change Canada (WVW), the Canada Foundation for Innovation (LC) and the Natural Sciences and Engineering Research Council of Canada (Discovery Grant to LC and Vanier Graduate Scholarship to WK), the University of Waterloo (WVW), and the University of Ottawa (WVW, LC, WK). We also thank two anonymous reviewers and the Canadian Journal of Remote Sensing editors for their input on this work.

ORCID

Wesley Van Wychen http://orcid.org/0000-0002-4275-6768
Will Kochtitzky http://orcid.org/0000-0001-9487-1509
Natalija Nikolic http://orcid.org/0000-0003-0128-1812
Luke Copland http://orcid.org/0000-0001-5374-2145

References

Abe, T., and Furuya, M. 2015. "Winter speed-up of quiescent surge-type glaciers in Yukon, Canada." *The Cryosphere*, Vol. 9(No. 3): pp. 1183–1190. doi:10.5194/tc-9-1183-2015.

Allen, C. 2013. *Icebridge MCoRDS L3 gridded ice thickness, surface, and bottom, Version 2.* Boulder, CO: NASA National Snow and Ice Data Center Distributed Active Archive Center.

Box, J.E., Colgan, W.T., Wouters, B., Burgess, D.O., O'Neel, S., Thomson, L.I., and Mernild, S.H. 2018. "Global sea-level contributions from Arctic land ice: 1971-2017." *Environmental Research Letters*, Vol. 13(No. 12): pp. 125012. doi:10.1088/1748-9326/aaf2ed.

Burgess, E., Forster, R., and Larsen, C. 2013. "Flow velocities of Alaska glaciers." *Nature Communications*, Vol. 4(No. 1): Article ID 2146. doi:10.1038/ncomms3146.

Burgess, D., Sharp, M., Mair, D., Dowdeswell, J., and Benham, T. 2005. "Flow dynamics and iceberg calving

rates of Devon Ice Cap, Nunavut, Canada." *Journal of Glaciology*, Vol. 51(No. 173): pp. 219–230. doi:10.3189/172756505781829430.

Ciracì, E., Velicogna, I., and Swenson, S. 2020. "Continuity of the mass loss of the world's glaciers and ice caps from the GRACE and GRACE follow-on missions." *Geophysical Research Letters*, Vol. 47((No. 9): pp. e2019GL086926. doi:10.1029/2019GL086926.

Cook, A., Copland, L., Noël, B., Stokes, C., Bentley, M., Sharp, M., Bingham, R., and Van den Broeke, M. 2019. "Atmospheric forcing of rapid marine-terminating glacier retreat in the Canadian Arctic Archipelago." *Science Advances*, Vol. 5(No. 3): pp. eaau8507. doi:10.1126/sciadv.aau8507.

Copland, L., Sharp, M., and Dowdeswell, J. 2003. "The distribution and flow characteristics of surge-type glaciers in the Canadian High Arctic." *Annals of Glaciology*, Vol. 36 pp. 73–81. doi:10.3189/172756403781816301.

Dalton, A., Copland, L., Tivy, A., Van Wychen, W., and Cook, A. 2019. "Iceberg production and characteristics around the Prince of Wales Icefield, Ellesmere Island, 1997–2015." *Arctic, Antarctic, and Alpine Research*, Vol. 51(No. 1): pp. 412–427. doi:10.1080/15230430.2019.1634442.

Danielson, B., and Sharp, M. 2013. "Development and application of a time-lapse photograph analysis method to investigate the link between tidewater glacier flow variations and supraglacial lake drainage events." *Journal of Glaciology*, Vol. 59(No. 214): pp. 287–302. doi:10.3189/2013JoG12J108.

Dowdeswell, J.A., Benham, T.J., Gorman, M.R., Burgess, D., and Sharp, M. 2004. "Form and flow of the Devon Island ice cap, Canadian Arctic." *Journal of Geophysical Research: Earth Surface*, Vol. 109(No. F2): pp. 1–14. doi:10.1029/2003JF000095.

GlaThiDa Consortium. 2019. *Glacier Thickness Database 3.0.1*. Zurich, Switzerland: World Glacier Monitoring Service.

Harcourt, W., Palmer, S., Mansell, D., Le Brocq, A., Bartlett, O., Gourmelen, N., Tepes, P., Dowdeswell, J., Blankenship, D., and Young, D. 2020. "Subglacial controls on dynamic thinning at Trinity-Wykeham Glacier, Prince of Wales Ice Field, Canadian Arctic." *International Journal of Remote Sensing*, Vol. 41(No. 3): pp. 1191–1213. doi:10.1080/01431161.2019.1658238.

Hattersley-Smith, G. 1964. "Rapid advance of glacier in northern Ellesmere Island." *Nature*, Vol. 201(No. 4915): pp. 176–176. doi:10.1038/201176a0.

Hattersley-Smith, G. 1969. "Recent observations on the surging Otto Glacier, Ellesmere Island." *Canadian Journal of Earth Sciences*, Vol. 6(No. 4): pp. 883–889. doi:10.1139/e69-090.

Jeffries, M. 1984. "Milne Glacier, Northern Ellesmere Island, N.W.T., Canada: A surging glacier?" *Journal of Glaciology*, Vol. 30(No. 105): pp. 251–253. doi:10.3189/S0022143000006043.

Mattar, K.E., Vachon, P.W., Geudtner, D., Gray, A.L., Cumming, I.G., and Brugman, M. 1998. "Validation of alpine glacier velocity measurements using ERS Tandem-Mission DAR data." *IEEE Transactions on Geoscience and Remote Sensing*, Vol. 36(No. 3): pp. 974–984. doi:10.1109/36.673688.

Medrzycka, D., Copland, L., Van Wychen, L., and Burgess, D. 2019. "Seven decades of uninterrupted advance of Good Friday Glacier, Axel Heiberg Island." *Journal of Glaciology*, Vol. 65(No. 251): pp. 440–452. doi:10.1017/jog.2019.21.

Millan, R., Mouginot, J., and Rignot, E. 2017. "Mass budget of the glaciers and ice caps of the Queen Elizabeth Islands, Canada, from 1991 to 2015." *Environmental Research Letters*, Vol. 12(No. 2): pp. 024016. doi:10.1088/1748-9326/aa5b04.

Mortimer, C., Sharp, M., and Van Wychen, W. 2018. Influence of recent warming and ice dynamics on glacier surface elevations in the Canadian High Arctic, 1995–2014. *Journal of Glaciology*, Vol. 64(No. 245): pp. 450–465. doi:10.1017/jog.2019.37.

RGI Consortium. 2017. "Randolph Glacier Inventory – A Dataset of Global Glacier Outlines: Version 6.0: Technical Report, Global Land Ice Measurements from Space, Colorado, USA." *Digital Media*. doi:10.7265/N5-RGI-60.

Rutishauser, A., Blankenship, D.D., Sharp, M., Skidmore, M., Greenbaum, J.S., Grima, C., Schroeder, D.M., Dowdeswell, J.A., and Young, D.A. 2018. "Discovery of a hypersaline subglacial lake complex beneath Devon Ice Cap." *Science Advances*, Vol. 4(No. 4): pp. eaar4353. doi:10.1126/sciadv.aar4353.

Sánchez-Gámez, P., and Navarro, F. 2017. "Glacier surface velocity retrieval using D-InSAR and offset tracking techniques applied to ascending and descending passes of sentinel-1 data for southern ellesmere ice caps." *Canadian Arctic, Remote Sensing*, Vol. 9(No. 5): pp. 442. doi:10.3390/rs9050442.

Schaffer, N., Copland, L., and Zdanowicz, C. 2017. "Ice velocity changes of Penny Ice Cap, Baffin Island, since the 1950s." *Journal of Glaciology*, Vol. 63(No. 240): pp. 716–730. doi:10.1017/jog.2017.40.

Schellenberger, T., Van Wychen, W., Copland, L., Kaab, A., and Gray, L. 2016. "An inter-comparison of techniques for determining velocities of maritime Arctic glaciers, Svalbard, using RADARSAT-2 Wide Fine mode data." *Remote Sensing*, Vol. 8(No. 9): pp. 785. doi:10.3390/rs8090785.

Shepherd, A., Du, Z., Benham, T., Dowdeswell, J., and Morris, E. 2007. "Mass balance of Devon Ice Cap, Canadian Arctic." *Annals of Glaciology*, Vol. 46 pp. 249–254. doi:10.3189/172756407782871279.

Short, N., and Gray, L. 2004. "Potential for RADARSAT-2 interferometry: glacier monitoring using speckle tracking." *Canadian Journal of Remote Sensing*, Vol. 30(No. 3): pp. 504–509. doi:10.5589/m03-071.

Short, N., and Gray, L. 2005. "Glacier dynamics in the Canadian High Arctic from RADARSAT-1 speckle tracking." *Canadian Journal of Remote Sensing*, Vol. 31(No. 3): pp. 225–239. doi:10.5589/m05-010.

Strozzi, T., Paul, F., Wiesmann, A., Schellenberger, T., and Kääb, A. 2017. "Circum-Arctic changes in the flow of glaciers and ice caps from satellite SAR data between 1990s and 2017." *Remote Sensing*, Vol. 9(No. 9): pp. 947. doi:10.3390/rs909047.

Thomson, L.I., Zemp, M., Copland, L., Cogley, J.G., and Ecclestone, M.A. 2017. "Comparison of geodetic and glaciological mass budgets for White Glacier, Axel Heiberg

Island." *Journal of Glaciology*, Vol. 63(No. 237): pp. 55–66. doi:10.1017/jog.2016.112.

Vachon, P.W., Geudtner, D., Mattar, K., Gray, A.L., Brugman, M., and Cumming, I. 1996. "Differential SAR interferometry measurements of Athabasca and Saskatchewan Glacier Flow Rate." *Canadian Journal of Remote Sensing*, Vol. 22(No. 3): pp. 287–296. doi:10.1080/07038992.1996.10855184.

Van Wychen, W., Copland, L., Gray, L., Burgess, D., Danielson, B., and Sharp, M. 2012. "Spatial and temporal variation of ice motion and ice flux from Devon Ice Cap, Nunavut, Canada." *Journal of Glaciology*, Vol. 58(No. 210): pp. 657–664. doi:10.3189/2012JoG11J164.

Van Wychen, W., Burgess, D., Gray, L., Copland, L., Sharp, M., Dowdeswell, J., and Benham, T. 2014. "Glacier velocities and dynamic ice discharge from the Queen Elizabeth Islands, Nunavut, Canada." *Geophysical Research Letters*, Vol. 41(No. 2): pp. 484–490. doi:10.1002/2013GL058558.

Van Wychen, W., Copland, L., Burgess, D., Gray, L., and Schaffer, N. 2015. "Glacier velocities and dynamic discharge from the ice masses of Baffin Island and Bylot Island, Nunavut, Canada." *Canadian Journal of Earth Sciences*, Vol. 52(No. 11): pp. 980–989. doi:10.1139/cjes-2015-0087.

Van Wychen, W., Davis, J., Burgess, D., Copland, L., Gray, L., Sharp, M., and Mortimer, C. 2016. "Characterizing interannual variability of glacier dynamics and dynamic discharge (1999-2015) for the ice masses of Ellesmere and Axel Heiberg Islands, Nunavut, Canada." *Journal of Geophysical Research – Earth Surface*, Vol. 121(No. 1): pp. 39–63. doi:10.1002/2015JF003708.

Van Wychen, W., Davis, J., Copland, L., Burgess, D., Gray, L., Sharp, M., Dowdeswell, J., and Benham, T. 2017. "Variability in ice motion and dynamic discharge from Devon ice Cap, Nunavut, Canada." *Journal of Glaciology*, Vol. 63(No. 239): pp. 436–449. doi:10.1017/jog2016.112.

Van Wychen, W., Copland, L., Jiskoot, H., Gray, L., Sharp, M., and Burgess, D. 2018. "Surface velocities of glaciers in Western Canada from Speckle-tracking of ALOS PALSAR and RADARSAT-2 data." *Canadian Journal of Remote Sensing*, Vol. 44(No. 1): pp. 57–66. doi:10.1080/07038992.2018.1433529.

Waechter, A., Copland, L., and Herdes, E. 2015. "Modern glacier velocities across the Icefield Ranges, St. Elias Mountains, and variability at selected glaciers from 1959 to 2012." *Journal of Glaciology*, Vol. 61(No. 228): pp. 624–634. doi:10.3189/2015JoG14J147.

Williamson, S., Sharp, M., Dowdeswell, J., and Benham, T. 2008. "Iceberg calving rates from northern Ellesmere Island ice caps, Canadian Arctic, 1999–2003." *Journal of Glaciology*, Vol. 54(No. 186): pp. 391–400. doi:10.3189/002214308785837048.